Journal of Polymers and the Environment (2020) 28:61–73
https://doi.org/10.1007/s10924-019-01581-1

ORIGINAL PAPER

# Development of Poly(lactic acid) Nanocomposites Reinforced with Hydrophobized Bacterial Cellulose

**Jhon Alejandro Ávila Ramírez[1,2,3] · Jimena Bovi[2,3,4] · Celina Bernal[3,4] · María Inés Errea[1] · María Laura Foresti[2,3]**

Published online: 18 October 2019


## Abstract

Poly(lactic acid)/bacterial cellulose nanocomposites were prepared by solvent casting. Aiming to reduce the incompatibility between polar bacterial cellulose (BC) and the nonpolar poly(lactic acid) (PLA) matrix which induces filler aggregation and poor reinforcement dispersion, BC was acetylated by the use of a non-conventional route catalyzed by citric acid. The derivatized BC (AcBC) was incorporated into de PLA matrix at varying filler loadings, and optical, morphological, structural, thermal, tensile and barrier (water vapor) properties of PLA/AcBC in comparison with PLA/BC were evaluated. Noticeable changes in the nanocomposite properties were ascribed to the success of the route proposed to surface hydrophobize BC, which significantly improved its dispersibility within the PLA matrix and the matrix-filler interaction. By the way, the variation of filler loading allowed attaining remarkable increases in the nanocomposite films stiffness without significant reductions in tensile strength and water vapor permeability.

**Keywords** Bacterial cellulose · Acetylation · Poly(lactic acid) · Nanocomposites · Filler content

## Introduction

In the last decades, the increasing consciousness of society on the limited availability of fossil fuel resources has promoted much interest on bio-based materials. At the same time, the large use and non-biodegradable character of traditional plastics derived from fossil fuels which have led to significant waste accumulation, has triggered extensive research on biodegradable polymers which under appropriate conditions will break down far more quickly [1]. Among them, poly(lactic acid) (PLA) is a biodegradable thermoplastic polyester totally produced from renewable resources and based on agricultural, biological, and chemical technologies [2, 3]. Advantageously, some of its properties such as high mechanical strength and stiffness, UV stability and gloss are comparable to those of many commodity polymers. Thus, in the last years, PLA has gained increasing attention in several fields of application, such as the automotive industry, medicine and packaging [4–6]. However, the lack of toughness, poor crystallization behavior and, sometimes, its low gas barrier properties or low thermal resistance, often limit PLA applications [6].

A well-established strategy to improve PLA properties is the development of composites with different reinforcements. Among them, due to their abundancy and renewable, biodegradable and non-toxic character, a variety of natural fibers and, more recently, several nanocellulosic substrates have been successfully used [7–9]. Cellulosic reinforcements with dimensions in the nanoscale usually display superior reinforcing capability due to their high aspect ratio and high stiffness of the crystal regions. In terms of nanocellulose availability and isolation methods, nanofibrillated and nanocrystalline celluloses are commonly obtained from

✉ María Laura Foresti
mforesti@fi.uba.ar

1 Centro de Ingeniería del Medio Ambiente (CIMA), Instituto Tecnológico de Buenos Aires (ITBA), Av. Eduardo Madero 399, CP 1106ACD Buenos Aires, Argentina

2 Grupo de Biotecnología y Materiales Biobasados, Instituto de Tecnología en Polímeros y Nanotecnología (ITPN-UBA-CONICET), Facultad de Ingeniería, Universidad de Buenos Aires, Las Heras 2214, CP 1127AAR Buenos Aires, Argentina

3 Consejo Nacional de Investigaciones Científicas y Técnicas (CONICET), Buenos Aires, Argentina

4 Grupo de Propiedades Mecánicas y Fractura, Instituto de Tecnología en Polímeros y Nanotecnología (ITPN-UBA-CONICET), Facultad de Ingeniería, Universidad de Buenos Aires, Las Heras 2214, CP 1127AAR Buenos Aires, Argentina

different vegetable sources by mechanical and/or chemical routes [10–12]. In addition, nanofibrillated cellulose in the form of nanoribbons can be obtained in fermentation processes mediated by specific bacteria [13, 14]. In contrast to plant cellulose, bacterial cellulose (BC) is devoid of macromolecules such as lignin or hemicellulose, and it is recognized for its ribbon-shaped fine fiber network structure, high crystallinity, high water-holding capacity, distinguished mechanical properties and good strength-to-weight ratio [5, 15].

Even if PLA/nanocellulose nanocomposites have widely been prepared using different processing techniques such as casting/evaporation and melt compounding, the incompatibility between cellulose and hydrophobic PLA is still a challenge which needs to be addressed. Compatibilization of PLA with nanocellulosic substrates can be achieved by physical adsorption of surfactants or polyelectrolytes [16, 17], polymer grafting [18–21] and chemical modification of nanocellulose by for example silylation or esterification [22–24]. In particular, acetylation of both nanofibrillar and nanocrystalline celluloses has been often performed to improve their compatibility with PLA. With this aim, the main target of most derivatization strategies available in the literature has been to keep the ultrastructure of nanocellulose intact and to hydrophobize only its surface [25–30], being perchloric and sulfuric acids the catalysts most often used with this purpose. Additionally, our group has previously assayed the acetylation of bacterial nanocellulose in presence of citric acid, confirming surface hydrophobization with tunable derivatization extent [31, 32]. The resulting surface acetylated BC samples were recently assayed as reinforcement of PLA, evidencing clear improvements in the nanofiller dispersibility and derived properties as a consequence of BC hydrophobization. With the reinforcement percentage assayed (3 wt%) the stiffness of the nanocomposites showed an increase of about 15% with respect to PLA reinforced with pristine BC [33]. With basis on the previous findings, in the current contribution, microbial nanocellulose acetylated in the presence of citric acid to a degree of substitution (DS) of 0.49 is used as reinforcement of PLA at varying loadings, aiming to prepare bio-nanocomposites with further improved mechanical profile. The effect of reinforcement content on the morphological, optical, structural, thermal, mechanical and barrier (water vapor) properties is particularly analyzed.

## Materials and Methods

### Materials

Commercial PLA (Nature Works®, trade name 3051D) with a molar mass of *ca.* $1.42 \times 10^4$ g/mol and a density of 1.24 g/cm$^3$ [34] was used as the matrix of the nanocomposites. Polymer pellets were dried under vacuum at 98 °C for 3 h before use.

Anhydrous dextrose (Biopack), yeast extract (Britania, Laboratorios Britania S.A.), meat peptone (Britania, Laboratorios Britania S.A.), citric acid (Merck), disodium phosphate (Anedra), glycerol (Sintorgan) and corn steep liquor (Ingredion), were all part of the formulation of BC fermentation medium. Acetic anhydride (Cicarelli), acetic acid (Cicarelli), chloroform (Cicarelli), citric acid (Merck) and acetone (Sintorgan) were used for BC acetylation and nanocomposites preparation. All other chemicals were of analytical grade and were utilized as received without further purification.

### Bacterial Cellulose Production

Bacterial cellulose (BC) was produced by the bacterial strain *G. xylinus* NRRL B-42 in static culture and under conditions optimized in a previous work [35]. The bacterial inoculum was previously cultured in 100 mL Erlenmeyers flasks with 20 mL of Hestrin and Schramm (HS) medium [36] and incubated with orbital agitation (200 rpm) at 28 °C for 48 h.

For BC production, 1% (v/v) inocula were transferred to 10 L steel trays containing 5 L of fermentation medium with 4% (w/v) glycerol and 8% (w/v) corn steep liquor, and statically incubated at 28 °C. After 14 days, cellulose pellicles were harvested and thoroughly rinsed with distilled water to remove the remaining culture medium. The washed pellicles were then homogenized for 5 min in a blender with KOH solution 5% (w/v) and left in alkali for 14 h at room temperature. BC was finally rinsed with distilled water until neutralization. Field emission scanning electron microscopy (FESEM) images of BC revealed a network of twisting nanoribbons of 30–70 nm width and micrometric in length.

### Acetylation of Bacterial Cellulose

Previously homogenized BC pellicles (2.5 g dry weight) were solvent exchanged from water through acetic acid into acetic anhydride (20 mL each time). BC was then placed in a 500 mL glass flask equipped with a reflux condenser containing 250 mL of acetic anhydride and 1 g of citric acid (0.34 mmol/mmol AGU). The mixture was heated up to 120 °C and kept at this temperature for 3 h in a thermostatized oil bath under continuous magnetic agitation. After this period, the derivatized BC (AcBC) was filtrated under vacuum and exhaustively washed with ethanol and distilled water until neutrality of the wash waters. The BC esterification level achieved was quantified by heterogeneous saponification of properly dried samples as described elsewhere [37].

## PLA/BC and PLA/AcBC Nanocomposites Preparation

Nanocomposites were prepared by solvent casting. With this purpose, BC and AcBC aqueous suspensions were solvent exchanged first in acetone (twice) and then in chloroform (twice). After each solvent exchange suspensions were homogenized at 18,000 rpm using a handheld homogenizer (Ultra Turrax D160).The nanocellulose dispersions (BC and AcBC, both in chloroform) were then mixed with PLA previously dissolved in the same solvent at proper concentrations to attain final nanofiller contents in the nanocomposites of 3, 5 and 10 wt%. Suspensions were homogenized at 18,000 rpm for 15 min and finally casted onto 90 mm glass Petri dishes and dried for 48 h at RT. The films were then placed in a vacuum oven at 40 °C for 4 weeks before characterization. The obtained films had a nominal thickness of ≈250 µm. For comparison, a neat PLA film was also prepared. Films were named according to Table 1.

## Characterization of Nanofillers and Composites

### Field Emission Scanning Electron Microscopy (FESEM)

Drops of diluted aqueous suspensions of BC and AcBC were deposited on microscope glasses and dried at 100 °C for 5 min. For the PLA/BC nanocomposites cryo-fractured surfaces obtained at liquid nitrogen temperature for the different samples were analyzed in a Zeiss Supra 40 microscope at an accelerating voltage of 3 kV. All samples were sputtered coated with a thin layer of gold before observation.

### Fourier Transform Infrared Spectroscopy (FTIR)

Fourier transform infrared spectra of reinforcements (BC and AcBC) were collected with an IR Affinity-1 Shimadzu Fourier Transform Infrared Spectrophotometer in absorbance mode. Carefully dried (12.5 mg, 110 ºC, 1 h) powdered samples were mixed with previously dried KBr (130 °C, overnight) at 1:20 ratio and pressed into a disc. The IR spectra were recorded between 4000 and 900 $cm^{-1}$ with 40 scans at a resolution of 4 $cm^{-1}$. Spectra were baseline corrected and normalized against the intensity of the absorption at 1165 $cm^{-1}$ corresponding to the (C–O–C) link of cellulose [27, 38].

**Table 1** Nanocomposite formulations

| System | PLA (wt%) | BC (wt%) | AcBC (wt%) |
|---|---|---|---|
| PLA | 100 | – | – |
| PLA/3BC | 97 | 3 | – |
| PLA/5BC | 95 | 5 | – |
| PLA/10BC | 90 | 10 | – |
| PLA/3AcBC | 97 | – | 3 |
| PLA/5AcBC | 95 | – | 5 |
| PLA/10AcBC | 90 | – | 10 |

### Solid-State Nuclear Magnetic Resonance Spectroscopy (CP/MAS $^{13}C$ NMR)

High-resolution $^{13}C$ solid-state spectra of neat and acetylated BC were recorded using the ramp {1H} → {13C} CP/MAS pulse sequence (cross-polarization and magic angle spinning) with proton decoupling during acquisition. Experiments were carried out at RT in a Bruker Avance II-300 spectrometer equipped with a 4-mm MAS probe. The operating frequency for protons and carbons was 300.13 and 75.46 MHz, respectively. Glycine was used as an external reference for the $^{13}C$ spectra and to set the Hartmann-Hahn matching condition in the cross-polarization experiments. The recycling time varied from 5 to 6 s according to the sample. The contact time during CP was 2 ms for all of them. The SPINAL64 sequence (small phase incremental alternation with 64 steps) was used for heteronuclear decoupling during acquisition with a proton field H1H satisfying $\omega 1H/2\pi = YHH1H = 62$ kHz. The spinning rate for all the samples was 10 kHz.

### X-ray Diffraction Analysis (XRD)

X-ray diffraction patterns of neat and acetylated BC as well as those of PLA/BC and PLA/AcBC composites were collected in a Rigaku D/Max-C Wide Angle automated X-ray diffractometer with vertical goniometer, using Cu/Kα radiation source (0.154 nm) at 40 kV and 30 mA. Diffractograms were recorded in a 2θ interval of 10–40° at a step size of 0.02°. The crystallinity index of BC and AcBC samples was estimated by use of Segal's empirical equation [39]:

$$CI = \left(I_{002} - I_{am}\right)/I_{002} \times 100 \quad (1)$$

where $I_{002}$ corresponds to the maximum intensity of the 002 lattice diffraction and accounts for both crystalline and amorphous material, and $I_{am}$ is the intensity at $2\theta = 18°$ which represents amorphous material only. The crystallinity of the composite films was determined from the ratio of the crystalline peaks area to the total diffractogram area.

### Light Transmittance Analysis

Composite films were characterized in terms of contact transparency and by recording their light transmittance curve using a Shimadzu UV/visible spectrophotometer (Model UV-1650pc) in the range of 200–800 nm. Spectra were recorded in at least three different positions within the films.

### Differential Scanning Calorimetry (DSC)

Thermal properties of PLA and the composites were determined by DSC (Shimadzu DSC-60) using a heating/cooling/heating cycle. A first heating scan at 10 °C/min from 30 to 200 °C was applied. Samples were then kept at 200 °C for 2 min in order to erase any thermal history, further cooled from 200 to − 25 °C at 10 °C/min, and finally heated again from − 25 to 200 °C at 10 °C/min. Crystallization ($T_c$), cold crystallization ($T_{cc}$) and melting ($T_m$) temperatures were determined as the maximum of the exothermic and endothermic signals, respectively. Glass transition temperature values ($T_g$) were obtained from cooling scans. The degree of crystallinity of the casted films was calculated according to Eq. (2), where $w_{PLA}$ is the weight fraction of PLA in the sample, $\Delta H_m$ is the melting enthalpy determined from the area of the endothermic peak of the first heating cycle,and $\Delta H_{m0}$ is the melting enthalpy for a 100% crystalline PLA taken as 93.7 J/g [40, 41]:

$$X = \left(1/W_{PLA}\right)(\Delta H_m/\Delta H_{mo}) \times 100 \quad (2)$$

### Uniaxial Tensile Tests

Uniaxial tensile tests were performed on dumbbell samples (at least five per system) cut out from the PLA matrix and the PLA/BC and PLA/AcBC composites films in an INSTRON dynamometer 5982. Stress–strain curves were obtainedat 1 mm/min and using a load cell of 1 KN in accordance with the ASTM D638 standard. From these tests average Young's modulus, tensile strength, and strain at break and their deviations were calculated.

### Water Vapor Permeability (WVP)

The water vapor transmission rate (WVTR) of the materials was determined following ASTM E96/E 96 M-05 (Desiccant method) whenever possible. Briefly, samples were sealed to the open mouth of acrylic test dishes (test area = $3.8 \times 10^{-4}$ $m^2$) containing silica gel (0% relative humidity) as desiccant, and the assemblies were placed in a chamber with controlled atmosphere at 24 °C and 53% relative humidity, the latter achieved by use of saturated solution of magnesium nitrate. Periodic weighings performed during 10 days allowed determination of the rate of water vapor movement through the films into the desiccant. Three specimens of each sample were tested by the same method.

Weight data collected over time was plotted against the elapsed time and the rate of water vapor transmission was determined from the slope of the straight line fitting the first points of the plot (Kg/s) divided by the test area ($m^2$). Water vapor permeability (WVP, Kg/msPa) was then determined from Eq. (3):

$$WVP = WVTR/\Delta p \times d = WVTR/(S \times (R1 - R2)) \times d \quad (3)$$

where WVTR is the rate of water vapor transmission (Kg/$m^2$s), $\Delta p$ is the vapor pressure difference (Pa), $S$ is the saturation vapor pressure at the test temperature (Pa), $R1$ is the relative humidity at the chamber expressed as a fraction, $R2$ is the relative humidity at the vapor sink expressed as a fraction, and $d$ is the sample thickness (m).

## Results and Discussion

Characterization assays of derivatized BC evidenced that acetyl functional groups ($CH_3$–C=O) were effectively introduced onto BC nanoribbons, whereas saponification of AcBC indicated that a degree of substitution of 0.49 was attained. Esterification became evident from FTIR spectrum of AcBC (C=O and C–O stretching observed at 1745 $cm^{-1}$ and 1240 $cm^{-1}$ respectively, and C–H bending at 1368 $cm^{-1}$) (Fig. 1a); and from new resonances characteristic of acetyl groups that emerged in the high-resolution $^{13}C$ solid-state NMR spectrum of AcBC (methyl carbons at 21 ppm and carbonyl carbons of the acetate groups at 171.5 ppm) (Fig. 1b). No resonance characteristic of citric acid/citrate ester was observed at ≈44 ppm.

FESEM images of BC and AcBC are shown in Fig. 1c, with their characteristic nanometric-in-width and micrometric-in-length intertwined ribbons. The morphology and dimensions of bacterial cellulose was conserved upon derivatization with no visible damage on the fibrils surface. The similarity between neat BC and AcBC X-ray diffraction patterns (typical cellulose I structure with three well-defined diffraction peaks centered at 2θ = 14.4° (101), 16.7° (10-1) and 22.6° (002) (Fig. 1d)), as well as their corresponding CI values calculated by Segal's empirical method (92% for BC and 91% for AcBC), suggested surface-only derivatization, which was actually the target aiming to avoid cellulose ultrastructure modification. Confinement of BC acetylation to the nanofibers surface or to their more accessible amorphous cellulose domains, is highly desirable to avoid affecting crystalline regions of the inner layers of cellulose fibers and their main mechanical and morphological properties [29]. Main characterization data for BC and AcBC are summarized in Fig. 1.

BC and AcBC were then used at 3, 5 and 10 wt% to prepare PLA/BC and PLA/AcBC composites by solvent casting. Figure 2 contains representative photographs of the films obtained. The quality of filler dispersion in the PLA matrix was visually evaluated in terms of the transparency of the resulting films, since if the reinforcement is not in the nanoscale (i.e. aggregated nanofibers), the light transmittance of the material decreases due to the increased light scattering [42]. In Fig. 2, whereas the neat PLA film looks homogeneous and the characteristic transparency of neat PLA films is recognized, incorporation of pristine BC results

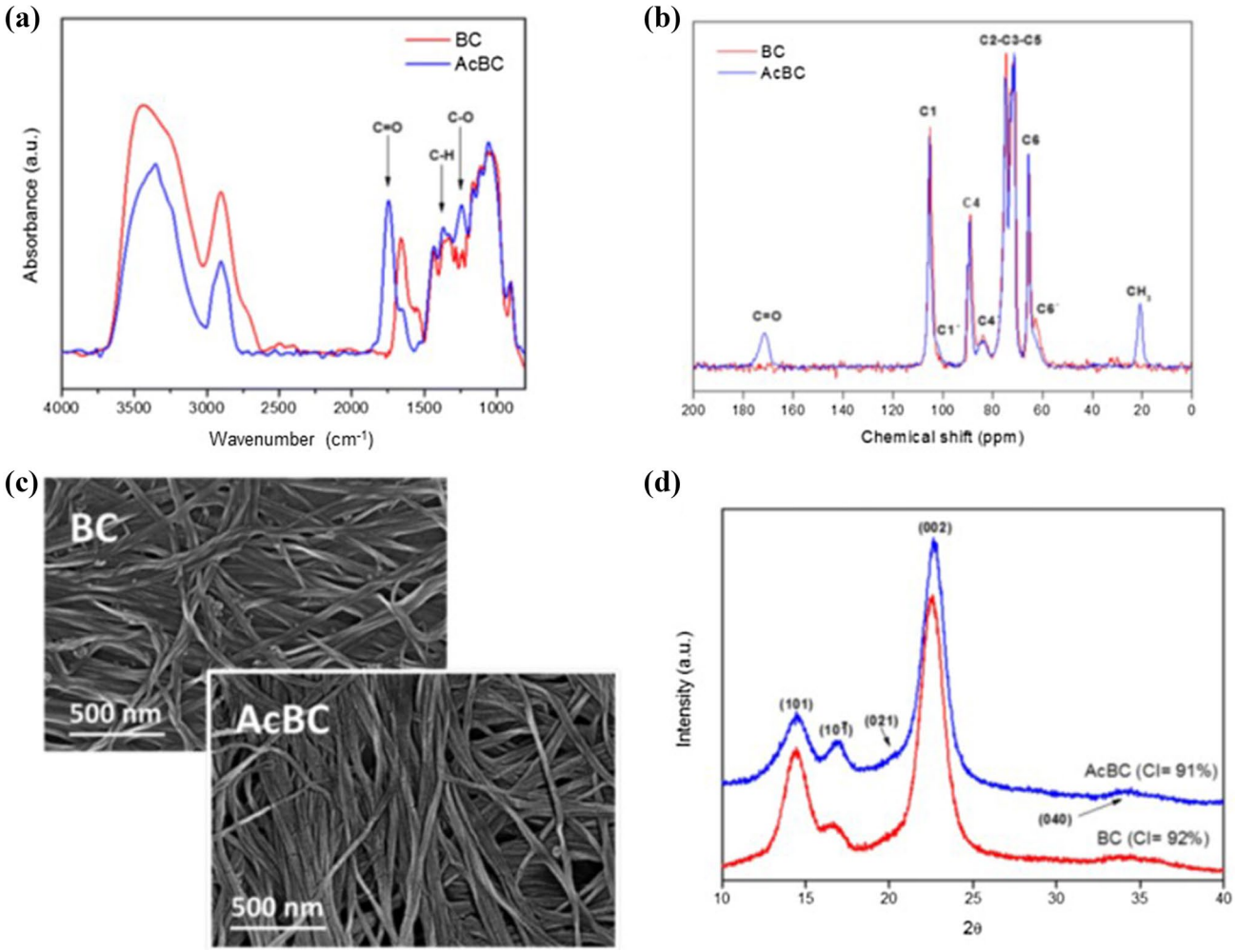


**Fig. 1** BC and AcBC main characterization. **a** FTIR spectra, **b** $^{13}C$ solid-state NMR spectra, **c** FESEM micrographs and **d** XRD patterns

in films less traslucent in which nanofiller aggregates are clearly evident to the naked eye, even for the lowest BC percentage assayed. The previous is associated with the well-known incompatibility of BC and less polar PLA, which promotes nanofibers aggregation and hinders their proper dispersion within the polymeric matrix. As it was expected, the addition of higher BC contents (i.e. 5 and 10 wt%) was accompanied by more visible reductions in films transparency. The qualitative observations described before are further supported by light transmittance data (Fig. 3), which illustrate the progressive reduction of transmittance in the whole wavelength interval assayed as a result of the incorporation of higher unmodifed BC loadings into the PLA matrix.

On the other hand, PLA/AcBC nanocomposites were much more homogenous, with noticeable improvements in transparency with respect to the counterparts involving unmodified BC. Similar observations were previously described for composites of PLA containing unmodified microfibrillated cellulose (MFC) of plant origin which were off-white in colorwith the appearance of MFC aggregates as white dots all over the film. In contrast, in the films with acetylated MFC as filler the presence of aggregates progressively vanished with the modification extent achieved, and the films became increasingly translucent, indicating significant improvement of MFC dispersion in the PLA film upon acetylation [43].

The transmittance curves of the films further illustrated the observations just made (Fig. 3). The data collected for the PLA/3AcBC film was actually very close to that of the neat PLA film, suggesting successful dispersion of nanoribbons within the matrix as a result of hydrophobization of their surface. Significant retention of the original neat PLA film transparency upon incorporation of surface acetylated BC pellicles has been previously attributed to bacterial cellulose presence in the form of nanosized fibrils, so that the nanocomposite is free from light scattering [44]. On the other hand, higher AcBC loadings (i.e. 5 and 10 wt%)

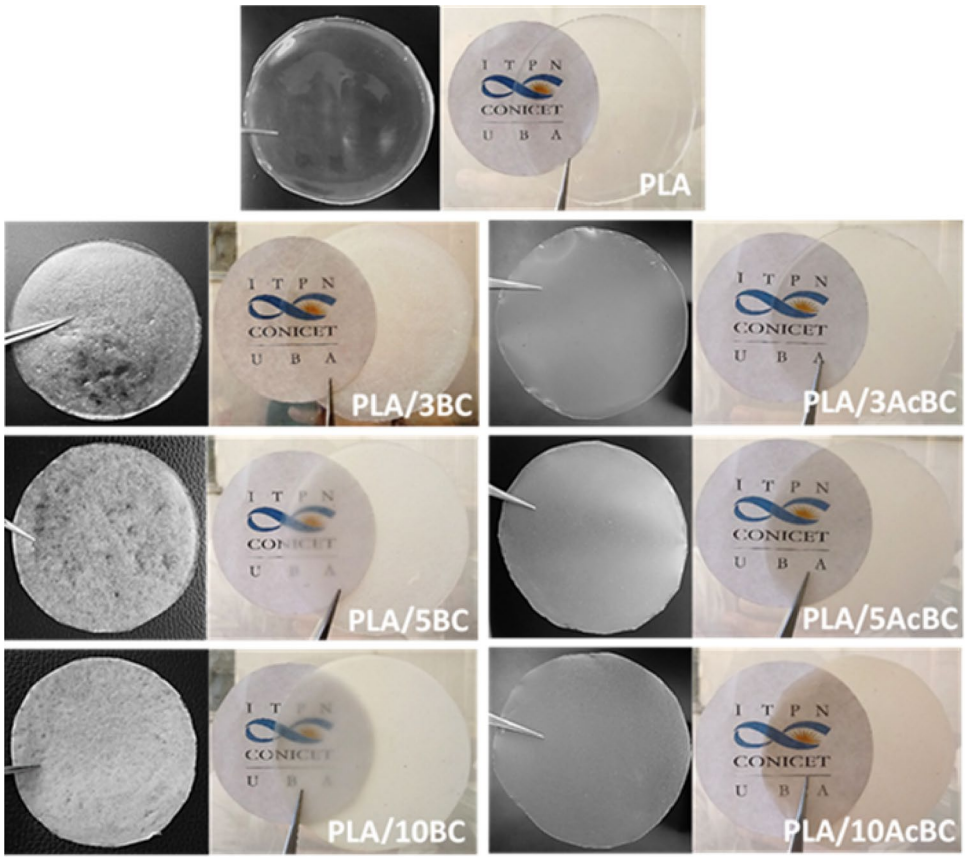


**Fig. 2** Photographs of neat PLA, PLA/BC and PLA/AcBC nanocomposites films with different nanofiller content illustrating their relative transparency

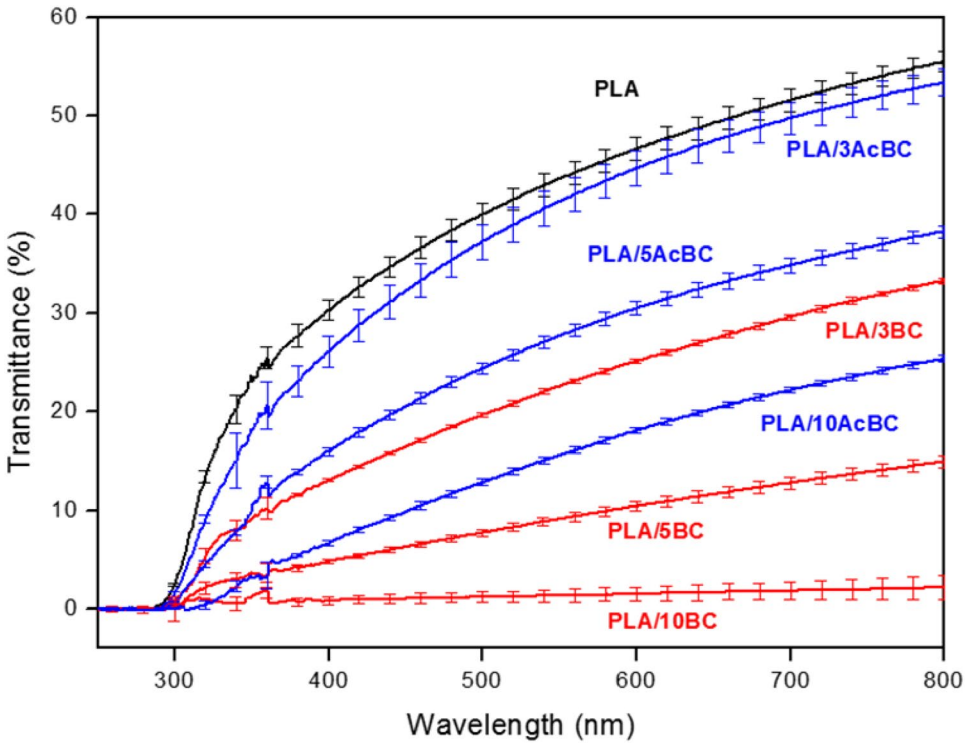


**Fig. 3** Light transmittance curves of neat PLA, PLA/BC and PLA/AcBC nanocomposite films

gradually reduced the films transparency, from which it may be infered that, despite acetylation, partial aggregation of BC took place for such filler contents promoting the scattering of light. In any case, qualitative and quantitative comparison of PLA/5AcBC and PLA/10AcBC with the nanocomposites containing equal amounts of neat BC undoubtedly highlighed the much better dispersion of BC nanoribbons in PLA achieved upon their surface hydrophobization. In this way, due to acetylation, significantly higher filler loadings could be used with a comparable concomitant transparency loss. Important improvements in nanofibrillated celluloses dispersion in PLA upon acetylation (achieved by other routes) have been previously reported [29, 45].

FESEM micrographs of cryogenic fracture surfaces of the different composites obtained are shown in Fig. 4. Irrespectively of the filler content, samples with AcBC presented more uniform fracture surfaces with less evidence of nanoribbons aggregation than samples with pristine BC, which exhibited voids around larger BC aggregates. Similar findings have been previously reported for PLA reinforced with

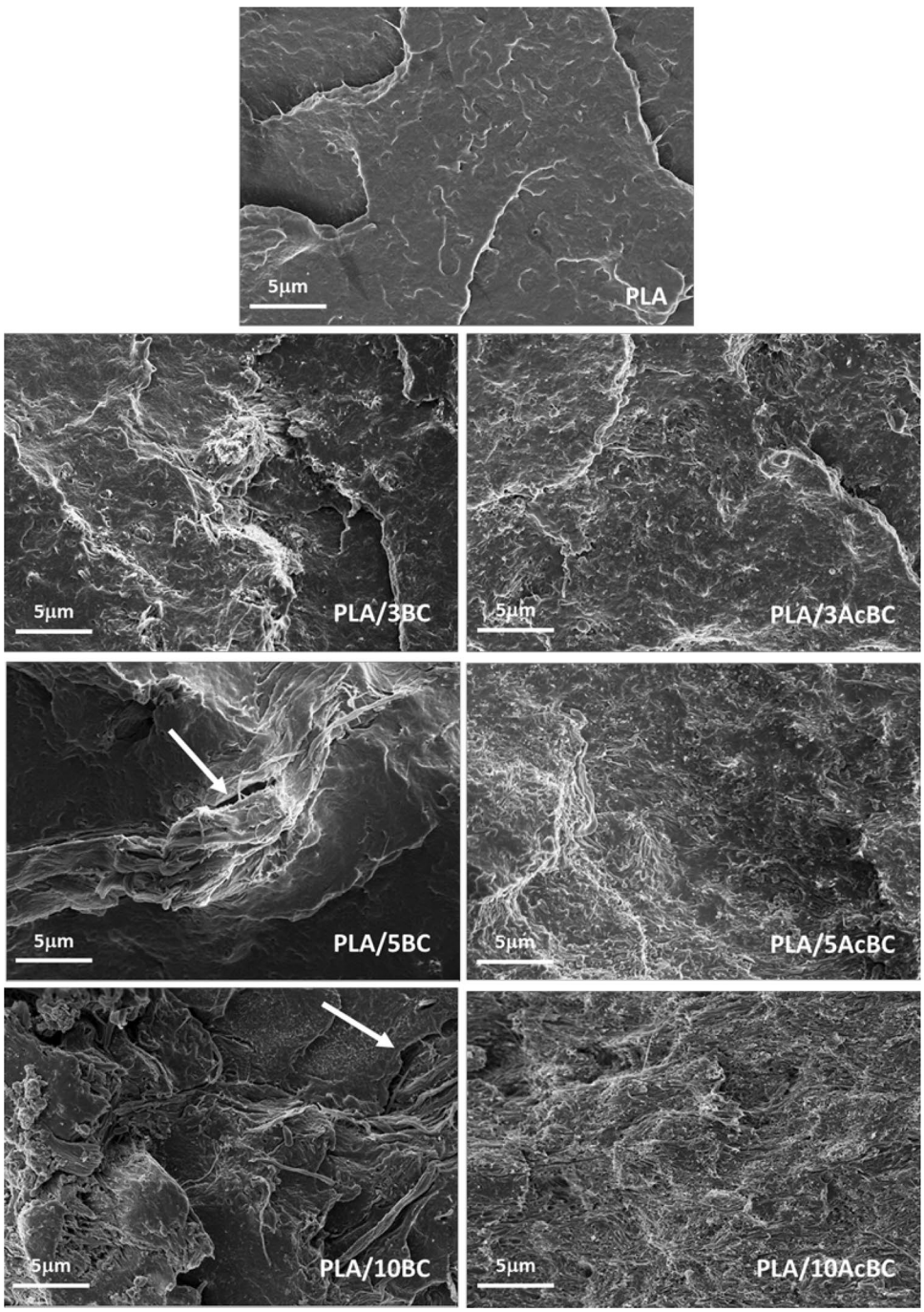


**Fig. 4** FESEM micrographs of cryogenic fracture surfaces of neat PLA, PLA/BC and PLA/AcBC nanocomposite films. White arrows point towards the voids around BC aggregates

microcrystalline cellulose which have been associated with poor adhesion between composite components [46]. The more homogeneous morphology presented by PLA/AcBC samples (better filler dispersion) can be attributed to the higher compatibility of BC with the PLA matrix achieved from derivatization, in agreement with observations previously reported for similar composites [29].

In addition to macroscopic and FESEM images of the films, BC and AcBC presence in the composites became also evident from XRD data. Figure 5 collects the X-ray diffractograms of the composite films with the highest nanocellulose content used, i.e. PLA/10BC and PLA/10AcBC. As it is shown, besides PLA strong crystalline peak at 2θ = 16.6° and its weaker peak at 19.1°, typical of semicrystalline PLAs [47, 48], composite diffractograms showed the presence of a crystalline peak at 22.3° associated with the (002) plane of bacterial cellulose. Even if PLA itself actually has a minor peak centered at 22.4°, the marked increase of its intensity upon incorporation of 10 wt% of BC or 10 wt% of AcBC is inarguable. Due to overlapping with crystalline signals of the PLA herein used, BC typical diffractions could not be identified at lower filler contents [33]. Conversely, XRD data from composites involving less crystalline PLAs have often evidenced the presence of typical BC crystalline peaks more clearly, especially as increasing nanofiller contents were assayed [44, 49]. According to XRD data, all materials investigated herein displayed crystallinity values within the 37–39% range.

Thermal properties of the different samples were analyzed from DSC data. First and second heating traces as well as cooling thermograms for neat PLA, PLA/BC and PLA/AcBC films are shown in Fig. 6, and key data are summarized in Table 2.

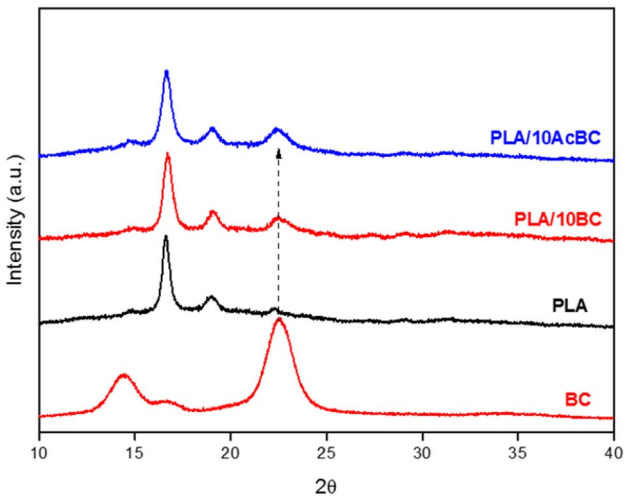


**Fig. 5** X-ray diffraction patterns of BC, neat PLA, PLA/10BC and PLA/10AcBC nanocomposite films

Upon first heating (Fig. 6a) all samples exhibited an endothermic melting peak with $T_m$ in the 149–152 °C interval, and $\Delta H_m$ values in the 30–33 J/g range (Table 2), globally indicating that no remarkable differences in the thermal behavior among the different materials obtained were observed. Crystallinity values calculated from first heating DSC data were found to be within the 32–36% interval, in quite good agreement with XRD results.

During the cooling scan, PLA showed no crystallization event at the cooling rate assayed. On the other hand, small exothermic peaks at 96–98 °C related to crystallization phenomena were observed for all composites containing pristine BC (Fig. 6b), which indicated that the addition of unmodified BC favored PLA crystallization. In fact, the magnitude of the crystallization event increased with the BC content (Table 2). The nucleating effect of BC on the crystallization of PLA has been already observed by others [44, 50]. However, crystallization upon cooling could not be detected in the nanocomposites containing acetylated BC. It has been reported in the literature that reinforcing fibers may not only act as nucleation sites for the crystallization of PLA, but also they may restrict the mobility of the polymer chains [41]. These two actions can always be present when the polymer is cooled in the presence of well-dispersed fibers. Herein, results suggest that when pristine BC is used as filler, nucleation is promoted; whereas in nanocomposites with AcBC this effect might have been counteracted by PLA chains inmobilization. $T_g$ values determined from the cooling scan were in all cases in the 58–59 °C range, in accordance with the values reported in the literature for this type of PLA [34].

During the second heating (Fig. 6c) neat PLA showed neither exothermic peak attributed to its cold crystallization nor crystals fusion events. Contrarily, all composites exhibited both cold crystallization and melting peaks at different temperatures and with varying intensity depending on whether BC or AcBC was used as filler. For PLA/BC composites a double melting behavior with one peak at ≈ 147–149 °C and a second one at ≈ 152–153 °C was observed. This phenomenon has been previously attributed to the presence of small and imperfect crystals or to lamellar species with different perfection degrees, which later change into more stable crystals through melting and recrystallization at low heating rates [51].The double melting peak behavior shown in Fig. 6c for PLA/BC has been previously observed in second heating scans of composites of PLA and unmodified sisal fibers. In the mentioned case, authors claimed that the presence of the two melting peaks were indicative of two crystal fractions (meta-stable and perfect crystals) formed during the original cooling of the sample and the subsequent cold crystallization [52]. The existence or not of those peaks underlines the difference in the ability to re-crystallize of the different composites. A higher

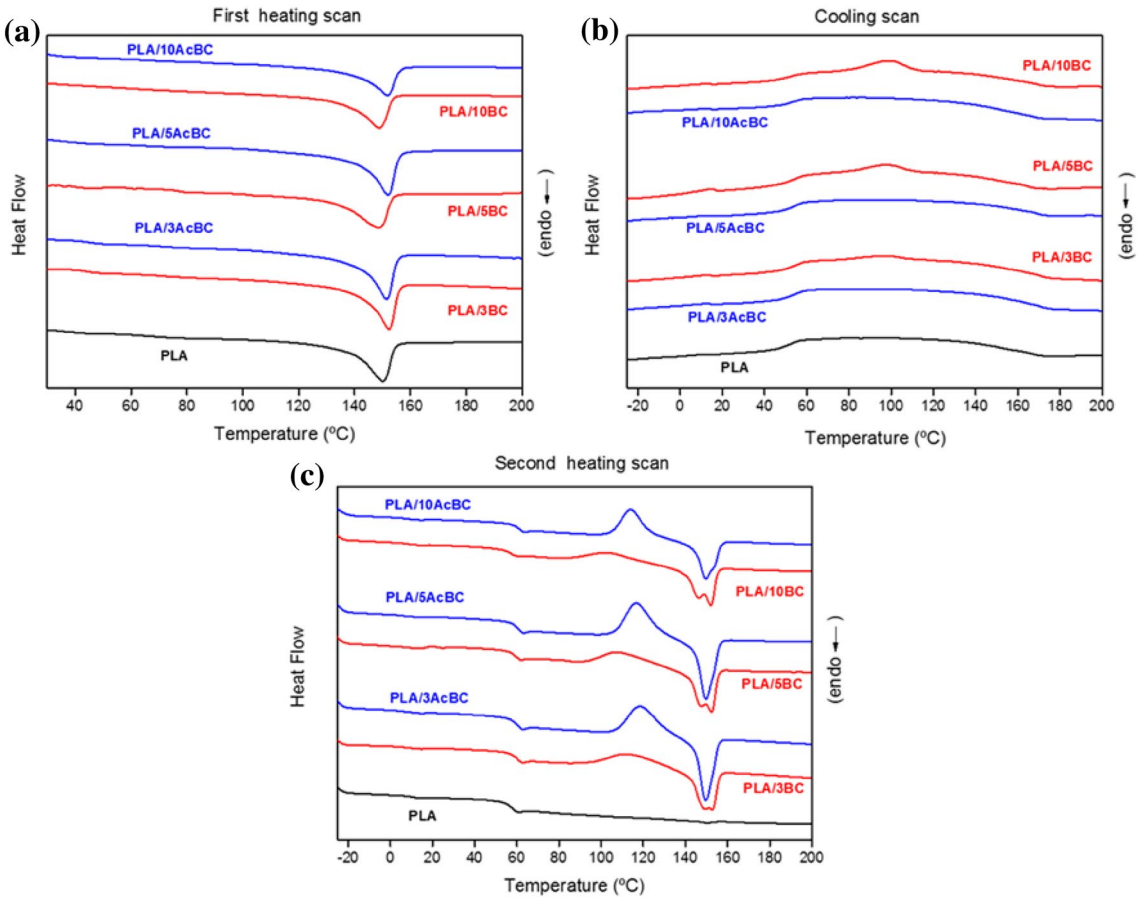


**Fig. 6** DSC thermograms of neat PLA, PLA/BC and PLA/AcBC nanocomposite films. **a** First heating scan **b** cooling scan, and **c** second heating scan

**Table 2** Thermal properties of PLA, PLA/BC and PLA/AcBC nanocomposite films

| Sample | First heating scan | | | Cooling scan | | | Second heating scan | | | |
|---|---|---|---|---|---|---|---|---|---|---|
| | $T_m$ (°C) | $\Delta H_m$ (J/g) | X (%) | $T_g$ (°C) | $T_c$ (°C) | $\Delta H_C$ (J/g) | $T_{cc}$ (°C) | $\Delta H_{CC}$ (J/g) | $T_m$ (°C) | $\Delta H_m$ (J/g) |
| PLA | 150 | 30 | 32 | 58 | – | – | – | – | – | – |
| PLA/3BC | 152 | 32 | 34 | 59 | 96 | 3 | 111 | 16 | 149; 153 | 21 |
| PLA/3AcBC | 152 | 33 | 35 | 59 | – | – | 118 | 23 | 150 | 24 |
| PLA/5BC | 149 | 33 | 36 | 59 | 96 | 6 | 108 | 13 | 147; 152 | 23 |
| PLA/5AcBC | 152 | 33 | 35 | 59 | – | – | 117 | 25 | 150 | 26 |
| PLA/10BC | 149 | 33 | 35 | 58 | 98 | 10 | 102 | 11 | 147; 152 | 24 |
| PLA /10AcBC | 152 | 32 | 34 | 58 | – | – | 114 | 18 | 150 | 21 |

molecular mobility of PLA in the presence of an incompatible filler like BC may justify the double melting behavior exhibited by the PLA/BC composites as a result of their better recrystallization ability. On the other hand, in samples containing AcBC the cold crystallization peak shifted to higher temperatures and a single melting behavior was observed. This could be attributed to the restricted mobility of polymer chains induced by the higher compatibility between PLA and acetylated BC. However, the existence of cold crystallization phenomena in PLA/AcBC nanocomposites (which were not present in neat PLA), suggested that AcBC fibers still acted as nucleating agents. Similar results regarding the effect of acetylation of BC on PLA crystallization have been previously reported [45].

In terms of mechanical properties, in uniaxial tensile tests neat PLA exhibited ductile behavior, whereas all composites

were much more brittle, in agreement with previous observations [33]. Tensile parameters values are presented as relative values with respect to neat PLA in Fig. 7. As it can be observed in this figure the incorporation of pristine BC into PLA led to a reduction in stiffness and strength, as a result of the important aggregation and deficient dispersion of the BC nanoribbons within the much less polar PLA matrix. In addition, poor interfacial adhesion between composite components reduced the ability to transfer stress from the matrix to the reinforcement, thereby limiting the tensile strength of the composites [53].

In contrast, functionalization of BC led to significantly improved filler dispersion and filler/matrix interaction. As a result, with the increase of the AcBC content the stiffness of the nanocomposites was remarkably improved (up to 40% with respect to neat PLA), while the tensile strength of the matrix was mantained. The improvement in the mechanical properties of nanocomposites has been related to the incorporation of a less compliant phase in the polymer matrix. In this case, part of the external stress is absorbed by the harder phase, while some is dissipated by particle–particle and particle-polymer friction [54]; provided proper nanofiller dispersion and reinforcement/matrix compatibility are achieved. The increasing trend in stiffness found with AcBC loading suggests that even at the highest filler content investigated (10 wt%), acetylated BC was still adequatly dispersed within the PLA matrix. Better filler dispersion and subsequent improvement in stiffness and strength values were previously reported for PLA reinforced with microfibrillated cellulose acetylated with a similar degree of substitution

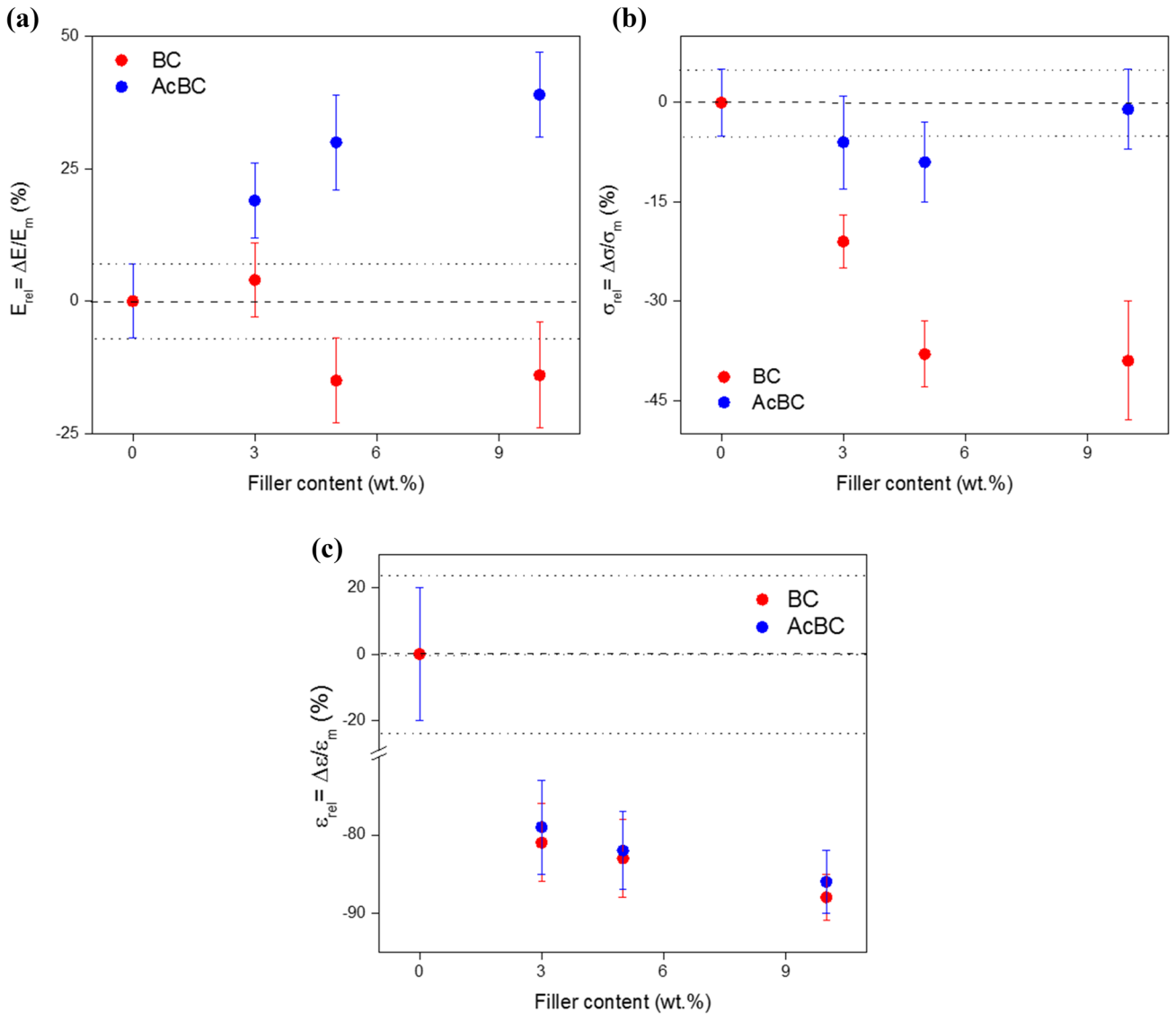


**Fig. 7** Tensile parameters values of PLA, PLA/BC and PLA/AcBC nanocomposite films presented as relative values with respect to neat PLA. **a** Young's modulus, **b** tensile strength, **c** strain at break

than the one conferred to BC in this work [55]; and also for PLA reinforced with other esterified bacterial celluloses [56].

Composites ductility, on the other hand, was significanlty reduced respect to neat PLA irrespectively of the filler surface chemistry, as expected from the introduction of a stiffer filler into a higher ductility matrix [57].

The results of tensile strength obtained herein were also analyzed in terms of the model proposed by Pukánszky et al. 1988 [58]. This model presents a quantitative evaluation of the composition dependence of composite strength, and it is able to determine the extent of interfacial interaction and detect the effect of filler aggregation. According to this model, the composite strength is determined by three components: the matrix strength, the effective load-bearing cross-section, and the interaction between phases. The simplified form of this model for small deformations is [59]:

$$\sigma = \sigma_o\left[(1-vf)/(1+2.5vf)\right] \times \exp(B\,vf) \quad (4)$$

where $\sigma$ and $\sigma_o$ are the tensile strength of the composite and the matrix, respectively; $vf$ is the filler volume fraction and $B$ is a parameter related to the filler load-bearing capacity. The parameter $B$can be obtained from the linear form of the above equation and, in general, a higher $B$ value indicates a stronger interfacial interaction [60]. Reduced composite strength can be expressed by rearranging Eq. (4):

$$\sigma_{red} = \sigma(1+2.5vf)\big/\left(\sigma_o(1-vf)\right) = \exp(B\,vf) \quad (5)$$

The natural logarithm of Eq. 5 should depend linearly on composition having a slope of $B$. The linear plot also allows to check the validity of the model and the presence of structural effects such as filler aggregation, as revealed from any deviation from a straight line.

The plot of the natural logarithm of reduced strength values as a function of BC or AcBC volume fraction is presented in Fig. 8. A rather good linear fit was obtained for the nanocomposites reinforced with acetylated BC. The $B$ parameter value was found to be 2.41 for these nanocomposites, which is in the same range of values reported in the literature for different PLA composites reinforced with lignocellulosic fibers [59, 61, 62]. For the composites with pristine BC, in contrast, all data points were scattered and completely deviated from a linear correlation, indicating the presence of some structural effects such as filler aggregation [63]. These results are in close agreement with the analysis of morphology by SEM, as well as with the results of light transmittance of the films (Figs. 4 and 3, respectively).

Finally, the water vapor permeability (WVP) of PLA and the composite films was assayed. Under the conditions used, the WVP of the neat PLA film was found to be $4.6\times10^{-13}\pm1.4\times10^{-14}$ kg/msPa, which is in the order of values previously reported for PLA [64]. Besides absolute values -which may actually vary with the type of PLA and

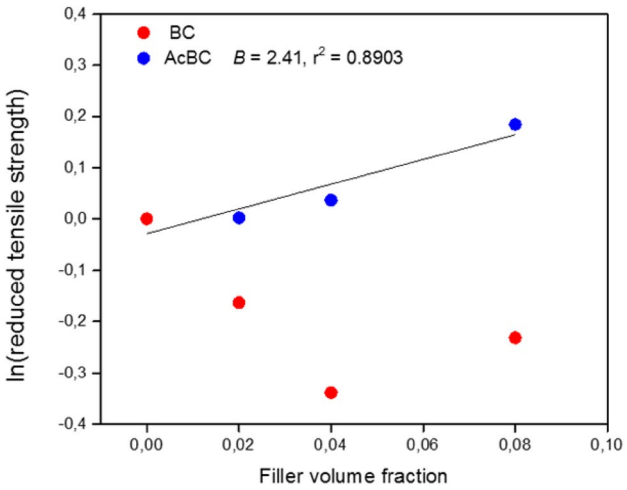


**Fig. 8** Natural logarithm of reduced tensile strength values as a function of filler volume fraction

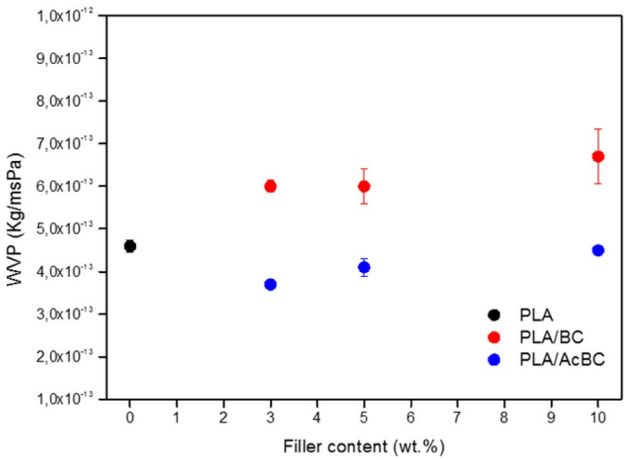


**Fig. 9** Water vapor permeability of neat PLA, PLA/BC and PLA/AcBC nanocomposite films

the assay conditions used-, data summarized in Fig. 9 clearly indicate that the addition of pristine BC increased the WVP values of the composites with respect to neat PLA, with relative change values in the order to those previously reported for this type of systems [65, 66]. The behavior (which was observed for all BC contents assayed) may be explained in terms of the addition of a filler with free surface hydroxyls groups which results in a strong incompatibility with the PLA matrix, both effects promoting water vapor transmission across the films.

Contrarily, the incorporation of acetylated BC resulted in a slight reduction in the WVP of the nanocomposite films with respect to the PLA matrix, especially for the PLA/3AcBC nanocomposite. This result again suggests a better dispersion of the nanofibers upon hydrophobization which may have allowed the formation of a finer nano-sized

fibrils network providing a more tortuous path to water vapor [64, 67]. Similar results have been previously reported for other PLA nanocomposites modified with cellulose nanofibers. In these composites, the addition of 1 and 3 wt% of pristine cellulose nanofibers led to increased WVP, whereas the addition of 1 and 3 wt% acetylated cellulose nanofibers not only improved the mechanical properties of the nanocomposites, but also allowed keeping the original permeability value of PLA due to a better distribution and high compatibility with the matrix [65]. On the other hand, the relatively higher WVP values shown in Fig. 9 for PLA/5AcBC and PLA/10AcBC may be explained in terms of partial aggregation of the nanofibers at such filler contents, which could have reduced the slight barrier effect attained when AcBC was incorporated at 3 wt%. These results are in agreement with the relative filler dispersion evidenced in Fig. 3 (light transmittance curves) for varying filler contents. Increasing WVP values at high cellulose nanofibrils loading has been often associated with filler aggregation providing channels or domains in the film that allow more rapid water permeation [66].

## Conclusions

In the current contribution, non-conventional sustainable acetylation of BC mediated by citric acid was carried out. Functionalized BC was used as reinforcement of PLA at varying filler contents and the optical, morphological, structural, thermal, mechanical and barrier properties of the composites were assayed as a function of the nanofibers load.

Comparison of characterization results obtained for PLA/AcBC with those of PLA/BC complementarily illustrated the compatibilization effect achieved upon acetylation of BC by the route proposed. Reduction of nanofibers polarity promoted better nanofiller dispersion within the hydrophobic PLA matrix, as clearly denoted by SEM micrographs and light transmittance analysis. Besides, the analysis of the effect of the filler content on the films transparency also indicated that at the lowest AcBC percentage assayed (i.e. 3 wt%) the light transmittance of neat PLA could be retained. On the other hand, whereas composites stiffness was significantly reduced by BC incorporation, the addition of AcBC resulted in significant increases in the Young's modulus of the films. In fact, the analysis of the effect of the AcBC content evidenced that by increasing it up to 10 wt% stiffness values $\approx$40% higher than that of the neat PLA matrix could be reached. Furthermore, in terms of the barrier properties of the films, the water vapor permeability of PLA was moderatly affected by the presence of the reinforcements, with higher WVP values when pristine BC was used as filler, and slight reductions in WVP with respect to neat PLA when the filler incorporated was AcBC. No evident effect of filler percentage could be inferred from WVP data. Finally, results also showed that the addition of the nanofibrillated microbial celluloses had a prominent role in inducing PLA crystallization, whose low crystallization rate is often a drawback for industrial applications. In this regard, the increased compatibility between the matrix and the esterified filler induced upon acetylation came also evident from significant modifications in the polymer crystallization behavior induced by restricted mobility of PLA chains upon improved fiber–matrix interaction.

Overall, optical, morphological, thermal, mechanical and water vapor barrier properties illustrated the better dispersability of BC within PLA achieved upon acetylation; whereas the evaluation of the filler content showed its prominent role in terms of the mechanical profile and the light transmittance of the nanocomposites.

**Acknowledgements** Authors acknowledge Consejo Nacional de Investigaciones Científicas y Técnicas (CONICET- PIP 11220150100660CO), University of Buenos Aires (UBACyT 20020170100696BA) and Agencia Nacional de Promoción Científica y Tecnológica (PICT 0843 2016 – PRESTAMO BID) for financial support.

## Compliance with Ethical Standards

**Conflict of interest** The authors confirm that this article content has no conflict of interest.

## References

1. Scaffaro R, Maio A, Sutera F, Gulino EF, Morreale M (2019) Polymers 11:651
2. Avérous L (2004) J Macromol Sci C 44:231
3. Jamshidian M, Tehrany EA, Imran M, Jacquot M, Desobry S (2010) Compr Rev Food Sci F 9:552
4. Avérous L (2008) In: Belgacem MN, Gandini A (eds) Monomers, polymers and composites from renewable resources, vol 1. Elsevier, Amsterdam, p 433
5. Petersen N, Gatenholm P (2011) Appl Microbiol Biot 91:1277
6. Panaitescu DM, Frone AN, Chiulan I (2016) Ind Crop Prod 93:251
7. John MJ, Thomas S (2008) Carbohydr Polym 71:343
8. Oksman K, Aitomäki Y, Mathew AP, Siqueira G, Zhou Q, Butylina S, Tanpichai S, Zhou X, Hooshmand S (2015) Composites A 83:2
9. Kian LK, Saba N, Jawaid M, Sultan MTH (2019) Int J Biol Macromol 121:1314
10. Nechyporchuk O, Belgacem MN, Bras J (2016) Ind Crop Prod 93:2
11. Ferreira FV, Mariano M, Rabel SC, Gouveia RF, Lona LMF (2018) Appl Surf Sci 436:1113
12. Pinheiro IF, Ferreira FV, Alves GF, Rodolfo A Jr, Morales AR, Mei LHI (2019) J Polym Environ 27:757
13. Iguchi M, Yamanaka S, Budhiono A (2000) J Mater Sci 35:261
14. Brown EE, Laborie MPG (2007) Biomacromol 8:3074
15. Berglund LA, Peijs T (2010) MRS Bull 35:201
16. Isogai A, Saito T, Fukuzumi H (2011) Nanoscale 3:71
17. Tardy BL, Yokota S, Ago M, Xiang W, Kondo T, Bordes R, Rojas OJ (2017) Curr Opin Colloid Int Sci 29:57

18. Goffin AL, Raquez JM, Duquesne E, Siqueira G, Habibi Y, Dufresne A, Dubois P (2011) Biomacromol 12:2456
19. Littunen K, Hippi U, Johansson LS, Österberg M, Tammelin T, Laine J, Seppälä J (2011) Carbohydr Polym 84:1039
20. Lonnberg H, Larsson K, Lindström T, Hult A, Malmström E (2011) ACS Appl Mater Interfaces 3:1426
21. Moon RJ, Martini A, Nairn J, Simonsenf J, Youngblood J (2011) Chem Soc Rev 40:3941
22. Johansson LS, Tammelin T, Campbell JM, Setälä H, Österberg M (2011) Soft Matter 7:10917
23. Missoum K, Belgacem MN, Bras J (2013) Materials 6:1745
24. Habibi Y (2014) Chem Soc Rev 43:1519
25. Kim DY, Nishiyama Y, Kuga S (2002) Cellulose 9:361
26. Nogi M, Abe K, Handa K, Nakatsubo F, Ifuku S, Yano H (2006) Appl Phys Lett 89:233123
27. Lee KY, Quero F, Blaker JJ, Hill CAS, Eichhorn SJ, Bismarck A (2011) Cellulose 18:595
28. Lin N, Huang J, Chang PR, Feng J, Yu J (2011) Carbohydr Polym 83:1834
29. Tomé LC, Pinto RJB, Trovatti E, Freire CSR, Silvestre AJD, Neto CP, Gandini A (2011) Green Chem 13:419
30. Cunha AG, Zhou Q, Larsson PT, Berglund LA (2014) Cellulose 21:2773
31. Ávila Ramírez JA, Gómez Hoyos C, Arroyo S, Cerrutti P, Foresti ML (2016) Carbohydr Polym 153:686
32. Ávila Ramírez JA, Gómez Hoyos C, Arroyo S, Cerrutti P, Foresti ML (2016) Curr Organocatal 3:161
33. Ávila Ramírez JA, Cerrutti P, Bernal C, Errea MI, Foresti ML (2018) J Polym Environ 27:510
34. Fortunati E, Armentano I, Zhou Q, Puglia D, Terenzi A, Berglund LA, Kenny JM (2012) Polym Degrad Stab 97:2027
35. Cerrutti P, Roldán P, Martínez García R, Galvagno MA, Vázquez A, Foresti ML (2016) J Appl Polym Sci 133:43109
36. Hestrin A, Schramm M (1954) Biochem J 58:345
37. Ávila Ramírez JA, Juan Suriano C, Cerrutti P, Foresti ML (2014) Carbohydr Polym 114:416
38. Ilharco LM, Gracia RR, da Silva JL, Ferreira LFV (1997) Langmuir 13:4126
39. Segal L, Creely JJ, Martin AE, Conrad CM (1959) Text Res J 29:786
40. Karim MN, Afroj S, Rigout M, Yeates SG, Carr C (2015) J Mater Sci 50:4576
41. Zhao LL, Su JJ, Han J, Zhanga B, Oua L (2017) RSC Adv 7:23065
42. Oksman K, Mathew AP (2014) In: Oksman K, Mathew AP, Bismarck A, Rojas O, Mohini S (eds) Handbook of green materials: processing technologies, properties and applications, vol 2. World Scientific, Singapore, p 53
43. Tingaut P, Zimmermann T, Lopez-Suevos F (2010) Biomacromol 11:454
44. Kim Y, Jung R, Kim HS, Jin HY (2009) Curr Appl Phys 9:S69
45. Zhang X, Li W, Ye B, Lin Z, Rong J (2011) J Thermoplast Compos Mater 26:346
46. Mathew AP, Oksman K, Sain M (2005) J Appl Polym Sci 97:2014
47. Wang Y, Funari SS, Mano JF (2006) Macromol Chem Phys 207:1262
48. Tábi T, Sajó IE, Szabó F, Luyt AS, Kovács JG (2010) Express Polym Lett 4:659
49. Ambrosio-Martın J, Fabra MJ, Lopez-Rubio A, Lagaron JM (2015) Cellulose 22:1201
50. Blaker JJ, Lee KY, Walters M, Drouet M, Bismarck A (2014) React Funct Polym 85:185
51. Fortunati E, Luzia F, Puglia D, Petrucci R, Kenny JM, Torre L (2015) Ind Crop Prod 67:439
52. Mofokeng JP, Luyt AS, Tábi T, Kovács J (2011) J Thermoplast Compos Mater 25:927
53. Jonoobi M, Harun J, Mathew AP, Oksman K (2010) Compos Sci Technol 70:1742
54. Ferreira FV, Dufresne A, Pinheiro IF, Souza DHS, Gouveia RF, Mei LHI, Lona LMF (2018) Eur Polym J 108:274
55. Bulota M, Kreitsmann K, Hughes M, Paltakari J (2012) J Appl Polym Sci 126:E448
56. Lee KY, Blaker JJ, Bismarck A (2009) Compos Sci Technol 69:2724
57. Pérez E, Famá L, Pardo SG, Abad MJ, Bernal C (2012) Compos Part B 43:2795
58. Pukánszky B, Turcsányi B, Tüdós F (1988) In: Ishida H (ed) Interfaces in polymer, ceramic and metal matrix composites. Elsevier, New York, p 467
59. Csikós A, Faludi G, Domján A, Renner K, Moczó J, Pukánszky B (2015) Eur Polym J 68:592
60. Demién Z, Pukánszky B, Nagy J (1998) Composites A 29:33
61. Csizmadia R, Faludi G, Renner K, Móczó J, Pukánszky B (2013) Composites A 53:46
62. Faludi G, Dora G, Imre B, Renner K, Moczó J, Pukánszky B (2014) J Appl Polym Sci 131:39902
63. Kiss A, Fekete E, Pukánszky B (2007) Compos Sci Technol 67:1574
64. Gårdebjer S, Larsson A, Löfgren C, Ström A (2014) J Appl Polym Sci 132:41219
65. Abdulkhani A, Hosseinzadeh J, Ashori A, Dadashi S, Takzare Z (2014) Polym Test 35:73
66. Almasi H, Ghanbarzadeh B, Dehghannya J, Entezami AA, Asl AK (2015) Food Packag Shelf Life 5:21
67. Song Z, Xiao H, Zhao Y (2014) Carbohydr Polym 111:442